Evidence of Ξ hypernuclear production in the $^{12}\text{C}(K^-,K^+)^{12}_{\Xi}\text{Be}$ reaction

P. Khaustov,[2] D. E. Alburger,[1] P. D. Barnes,[6] B. Bassalleck,[14] A. R. Berdoz,[2,*] A. Biglan,[2,†] T. Bürger,[11] D. S. Carman,[2,‡] R. E. Chrien,[1] C. A. Davis,[13,8] H. Fischer,[11] G. B. Franklin,[2] J. Franz,[11] L. Gan,[13,§] A. Ichikawa,[5] T. Iijima,[3] K. Imai,[5] Y. Kondo,[5] P. Koran,[2] M. Landry,[13] L. Lee,[13] J. Lowe,[10,14] R. Magahiz,[2,‖] M. May,[1] R. McCrady[2,¶] C. A. Meyer,[2] F. Merrill,[6] T. Motoba,[7] S. A. Page,[13] K. Paschke,[2] P. H. Pile,[1] B. Quinn,[2] W. D. Ramsay,[13] A. Rusek,[1] R. Sawafta,[1,**] H. Schmitt,[11] R. A. Schumacher,[2] R. W. Stotzer,[14,††] R. Sutter,[1] F. Takeutchi,[4] W. T. H. van Oers,[13] K. Yamamoto,[5] Y. Yamamoto,[9] M. Yosoi,[5] and V. J. Zeps[12]

(The AGS E885 Collaboration)

[1]*Brookhaven National Laboratory, Upton, New York 11973*
[2]*Carnegie Mellon University, Pittsburgh, Pennsylvania 15213*
[3]*KEK, High Energy Accelerator Research Organization, Tsukuba, Ibaraki 305, Japan*
[4]*Kyoto Sangyo University, Kyoto 603, Japan*
[5]*Kyoto University, Sakyo-Ku, Kyoto 606, Japan*
[6]*Los Alamos National Laboratory, Los Alamos, New Mexico 87545*
[7]*Osaka Electro-Communication University, Neyagawa, Osaka 572-8530, Japan*
[8]*TRIUMF, Vancouver, British Columbia, Canada V6T 2A3*
[9]*Tsuru University, Tsuru 402-8555, Japan*
[10]*University of Birmingham, Birmingham B15 2TT, United Kingdom*
[11]*University of Freiburg, D-79104 Freiburg, Germany*
[12]*University of Kentucky, Lexington, Kentucky 40507*
[13]*University of Manitoba, Winnipeg, Manitoba, Canada R3T 2N2*
[14]*University of New Mexico, Albuquerque, New Mexico 87131*

The E885 Collaboration utilized the 1.8 GeV/c K^- beam line at the Alternating Gradient Synchrotron (AGS) to accumulate greater than 10 times the world's existing data sample of (K^-,K^+) events on carbon. A total of about 3×10^5 (K^-,K^+) events were collected and analyzed. Ξ hypernuclear states are expected to be produced through the reaction $K^- + {}^{12}\text{C}\rightarrow K^+ + {}^{12}_{\Xi}\text{Be}$. A signal could also result from direct production of $^{11}_{\Lambda}\text{Be}+\Lambda$ without a distinct Ξ intermediate state. The measured missing-mass spectrum indicates the existence of a signal below the threshold for free Ξ^- production that cannot be explained by background or effects of limited resolution. Although the resolution was not sufficient to resolve discrete hypernuclear states, the excess of events in the region of missing mass, kinematically inaccessible in free Ξ^- production, can be compared with theoretical predictions for $^{12}_{\Xi}\text{Be}$ production. Reasonable agreement between the data and theory is achieved by assuming a Ξ-nucleus potential well depth $V_{0\Xi}$ of about 14 MeV within the Woods-Saxon prescription.

PACS number(s): 21.80.+a, 21.30.Fe, 25.80.Nv, 27.10.+h

I. INTRODUCTION

With the advent of magnetic spectrometers, it became possible to study hypernuclei through the reconstruction of missing mass. Hypernuclei with one strange quark ($S=-1$ sector) have long been studied using this method quite successfully. Similarly to production of $S=-1$ hypernuclei in

(π^+,K^+) and (K^-,π^-) reactions, the (K^-,K^+) reaction can be used to create $S=-2$ hypernuclei.

Dover and Gal found the Ξ-nucleus potential well depth to be $\approx$21–24 MeV based on their analysis of emulsion data [1]. The $1s$ and $1p$ single-particle Ξ^- states are expected to be bound for the values of the potential within that range. Although bound Ξ-nucleus states would be broadened by the conversion $\Xi N\rightarrow\Lambda\Lambda$, calculations have indicated that their widths could be a few MeV or less [2]. Fukuda *et al.* recently reported evidence for bound Ξ hypernuclei produced in the (K^-,K^+) reaction at $p_{K^-}=1.6$ GeV/c on a scintillating-fiber target (KEK E224) [3]. Their missing-mass resolution was not sufficient to resolve discrete hypernuclear states but their data seemed to favor a Ξ-nucleus potential well depth of $\approx$16 MeV. They concluded that a value of 24 MeV for the potential was improbable.

The 1.8 GeV/c K^- beam at the AGS was used to create doubly strange ($S=-2$) systems in E885 via the $^{12}\text{C}(K^-,K^+)\text{X}$ reaction at $p_{K^-}=1.8$ GeV/c. A high K^-
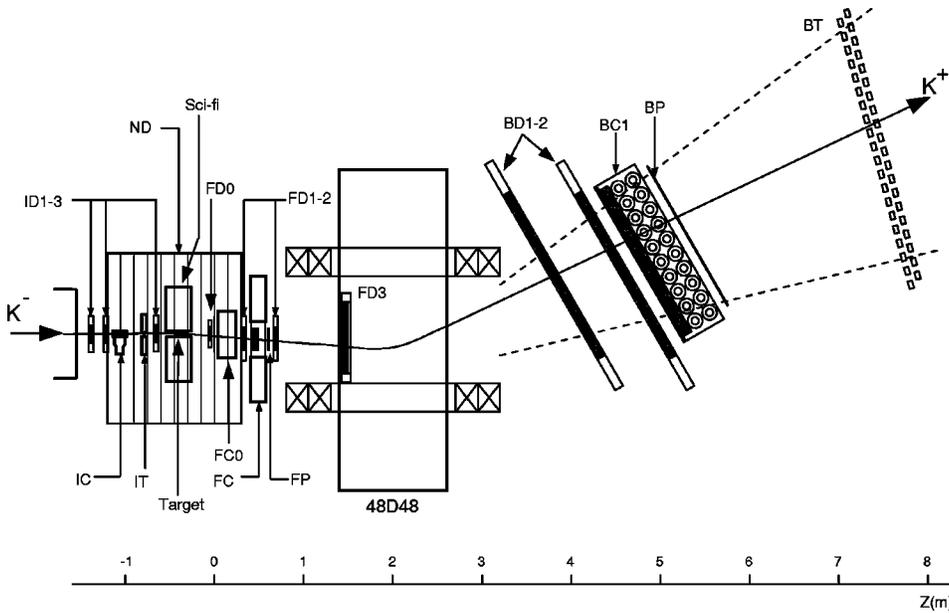
FIG. 1. Detector configuration for E885. The drift chambers ID1-3 determine the incident K^- trajectory and, combined with the beam line hodoscope MP (not shown here), the K^- momentum. The drift chambers FD0-3 and BD1-2 determine the K^+ trajectory through the 1.4 T 48D48 dipole. Scintillators IT and BT determine the K^+ time of flight. Hodoscopes FP and BP determine the spectrometer acceptance. Aerogel Cherenkovs IC, FC, and BC reject pions, while FC0 rejects protons. Above and below the target are scintillating fiber detectors. On the left and right of the target are neutron detectors. The fiber detectors and neutron detectors were not used in this analysis.

flux and a thick diamond target [4] combined to give a sensitivity to $S = -2$ states of 1.5 counts per nb/sr as compared to 0.05 counts per nb/sr for E224 [3]. Although the experimental resolution in E885 was somewhat better than the E224 resolution (4.2 MeV/c^2 rms vs 5.6 MeV/c^2 rms for hydrogen kinematics), it too was insufficient to resolve discrete hypernuclear states. Nevertheless, an estimate of the cross section can be made; the excitation-energy spectrum can be compared to the theoretical predictions for different potential well depths folded with our experimental resolution.[1]

The organization of this paper is as follows. In Sec. II the experimental setup for E885 is described and the event reconstruction is briefly discussed. In order to make cross section estimates and compare the data with theory, the missing-mass spectrum needs to be normalized. This normalization procedure is described in Sec. III. Prior to a comparison with our data, the theoretical cross section calculation must be folded with the experimental resolution function. The determination of the resolution function is described in Sec. IV. The theoretical cross sections for a series of values of the Ξ-nucleus potential well depth parameter, folded with the experimental resolution function, are compared with the data in Sec. V. A discussion of background is presented in Sec. VI, followed by our conclusions in Sec. VII.

II. EXPERIMENTAL SETUP

A side view of the E885 detector apparatus is shown in Fig. 1. The K^- beam was delivered by the AGS D6 beam line [5] at a rate of $10^6 K^-$/spill with a 1:1 K/π ratio. The

spill duration and repetition rate were 1.6 s and 1000 spills/hour, respectively (44% duty factor). The purity and intensity of the kaon beam provided by the AGS D6 beam line greatly exceeded that available elsewhere. The beam was focused in the vertical direction by the last beam line quadrupole magnet onto a synthetic diamond target, 8 cm wide $\times 1$ cm high $\times 5$ cm thick with a density of 3.3 g/cm^3. Diamond was used as the target material in order to enhance the Ξ^- stopping rate (a property not important for the direct production discussed in this paper); the resulting compactness of the target also allowed the application of tighter geometric cuts.

The momentum of the incident particle was measured using information from a scintillator hodoscope, MP, located in the beam line at the exit of the first mass slit (not shown in Fig. 1) and information from 3 drift chambers (ID1-3) located downstream of the last beam line magnet. The amplitude in the IC Cherenkov counter, along with the measured particle momentum and the beam line time of flight, were used to suppress triggers from pions. Additional details regarding the experimental apparatus can be found in Ref. [6].

The momentum of the outgoing K^+ was measured in the 1.4 T 48D48 magnetic spectrometer. The amplitude in the FC Cherenkov counter, along with the measured momentum and IT-BT time of flight, was used to select kaons. In addition to pions, protons were another source of background in the spectrometer. To reduce the hardware trigger rate, an aerogel Cherenkov counter, FC0, was used to suppress protons; its refraction index was selected to be sensitive to kaons but not protons from inelastic events. The measured mass spectrum for a sample of secondary particles is shown in Fig. 2. This shows that the kaons were cleanly separated from the pions and protons that passed the hardware triggers after goodness-of-fit and vertex cuts were applied. The pion peak in Fig. 2(a) is due to leakage of the hardware FC pion veto. These events were virtually eliminated by an additional software cut on FC pulse height. The results are shown in Fig. 2(b). The measured momenta of the incident and sec-

---

[1]Excitation energy E is defined as the missing mass minus the combined mass of the ^{11}B(g.s.) and the Ξ^- (all times c^2). With this definition the threshold for free Ξ^- production is at zero excitation energy and bound Ξ hypernuclear states have negative excitation energy.
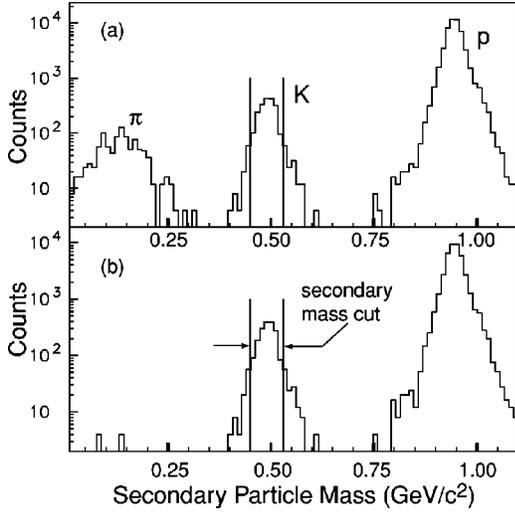
FIG. 2. The secondary particle mass as calculated from the measured momentum, path length, and time of flight through the K^+ spectrometer for a subset of the data. (a) Events that pass goodness-of-fit, vertex, and multiplicity cuts. (b) An additional software veto has been applied using the FC pulse height. Events in (b) that fall within the secondary-mass cut were used in the analysis.

ondary particles allow the calculation of the missing mass.

III. NORMALIZATION

Our data were normalized to the known forward-angle cross section of free Ξ^- production on hydrogen (contained in a CH_2 target). Due to the low statistics in the bound region, only angle-averaged differential cross sections could be obtained. These angle-averaged cross sections are denoted here as $\langle d^2\sigma/d\Omega dE \rangle$. We present results averaged over $0° < \theta_{K^+} < 14°$, corresponding to the full acceptance of the spectrometer, and for $0° < \theta_{K^+} < 8°$.

The normalization effectively scaled the diamond target results to agree with the Ξ^- production off carbon in a CH_2 target, which was, in turn, normalized to the Ξ production off hydrogen in the CH_2 target. This procedure corrected for differences in the event reconstruction efficiency between the low-intensity CH_2 running and the high intensity diamond target running. These differences were brought about, in part, by tight multiplicity cuts on detector MP.

The scale for the excitation-energy spectrum was set using the equation

$$\left\langle \frac{d^2\sigma}{d\Omega dE} \right\rangle^C = A \left(\frac{dN}{dE} \right)^C_{\text{diam}}, \tag{1}$$

where the normalization factor is given by

$$A = \frac{\alpha^H}{\alpha^C(E)} \frac{\lambda^H_{CH_2}}{\lambda^C_{CH_2}} \frac{N^C_{CH_2}}{N^C_{\text{diam}} N^H_{CH_2}} \left\langle \frac{d\sigma}{d\Omega} \right\rangle^H.$$

The following definitions were used.

$\langle d^2\sigma/d\Omega dE \rangle^C$: angle-averaged double-differential cross section for hypernuclear production on carbon.
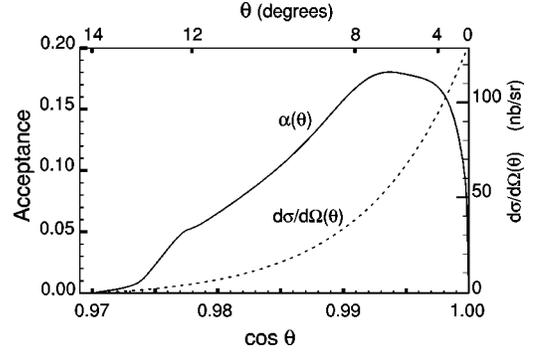

FIG. 3. The angular acceptance, $\alpha(\theta)$, generated by a Monte Carlo simulation is shown as the solid line. The dashed line shows the results of the DWIA calculation of the angular dependence of the cross section of the ground state using a potential depth of $V_{0\Xi} = 14$ MeV.

$(dN/dE)^C_{\text{diam}}$: number of hypernuclear-production events in an excitation energy interval dE from the diamond target.

α^H: angle- and energy-averaged acceptance for free Ξ^- production on hydrogen.

$\alpha^C(E)$: angle-averaged acceptance for hypernuclear production on carbon. The argument E indicates the dependence on excitation energy.

$\lambda^H_{CH_2}$: target thickness for hydrogen in CH_2 target.

$\lambda^C_{CH_2}$: target thickness for carbon in CH_2 target.

$N^C_{CH_2}$: number of events of free Ξ^- production on carbon in CH_2 target.

$N^H_{CH_2}$: number of events of free Ξ^- production on hydrogen in CH_2 target.

N^C_{diam}: number of events of free Ξ^- production on carbon in diamond target.

$\langle d\sigma/d\Omega \rangle^H$: angle-averaged differential cross section of Ξ^- production on hydrogen.

Since the spectrometer acceptance for hypernuclear production varies very little with energy over the small region of interest about zero excitation energy, instead of the energy-dependent acceptance $\alpha^C(E)$, the acceptance was calculated for a fixed excitation energy of -10 MeV. The angle-dependent acceptance used to determine $\alpha^C(E)$ was generated with a Monte Carlo simulation and is shown as the solid line in Fig. 3.

A summary of the parameters used for normalization in Eq. (1) is given in Table I for two different acceptances; the first one is full spectrometer acceptance ($\theta_{K^+} < 14°$) and the second is for limited acceptance ($\theta_{K^+} < 8°$)[2]. The following values for the normalization factor A, giving the angle-averaged differential cross section per event were obtained:

---

[2]Note that in both cases we use the value of 35 μb/sr for the elementary production cross section which is compatible with the measured value in Ref. [7]. This factor should be divided out when comparing these results to a calculation of the effective proton number.

TABLE I. A summary of parameters used for normalization. The value used for the cross section of Ξ^- production on hydrogen is compatible with the value measured by Iijima *et al.* [7].

Maximum θ_{K^+} (degrees)	α^{H}	$\alpha^{\mathrm{C}}(-10 \ \mathrm{MeV})$	$\lambda^{\mathrm{H}}_{\mathrm{CH_2}}/\lambda^{\mathrm{C}}_{\mathrm{CH_2}}$	$N^{\mathrm{C}}_{\mathrm{CH_2}}/N^{\mathrm{C}}_{\mathrm{diam}}$	$\langle d\sigma/d\Omega \rangle^{\mathrm{H}}$ (μ b/sr)	$N^{\mathrm{H}}_{\mathrm{CH_2}}$
14	8.1%	14.8%	2	1/125.6	35	480
8	14.4%	15.3%	2	1/127.9	35	240

$$A = \begin{cases} 0.64 \pm 0.05 \ \mathrm{nb/sr} \ \text{for} \ \theta_{K^+} < 14°, \\ 2.14 \pm 0.20 \ \mathrm{nb/sr} \ \text{for} \ \theta_{K^+} < 8°. \end{cases}$$

This factor relates the counts per MeV to the angle-averaged differential cross section per MeV. The statistical errors given for the normalizing factor A were due mostly to the limited amount of calibration data, namely the number of free Ξ^- production events on hydrogen and carbon in the $\mathrm{CH_2}$ target. The systematic uncertainty, excluding the uncertainty of the elementary cross section of Ξ^- production on hydrogen, is expected to be below the statistical error. The uncertainty of the elementary cross section for Ξ^- production on hydrogen does not affect the comparison between data and theory because the theoretical DWIA calculations are normalized to the same elementary cross section. Thus the data-to-theory ratio is insensitive to the assumed elementary cross section.

IV. MISSING-MASS RESOLUTION

Data sets were taken with two different $\mathrm{CH_2}$ targets and were used to study the missing-mass resolution. The first set used an 8 cm long target and the second set, which was acquired over a shorter time period, used a 13 cm long target. The first data set was used to study the spectrometer's intrinsic resolution and, in particular, to evaluate the tails of the resolution function. The second set was used to derive the width of the resolution function. The contribution of energy-loss effects to the resolution for the 13 cm long $\mathrm{CH_2}$ target is expected to be similar to the contribution from the 5 cm long diamond target.

Due to the two-body nature of Ξ^- production on hydrogen, the missing mass spectrum is a peak, whose width equals the experimental resolution, on top of a background from Ξ^- production on carbon. In addition to the peak width, we are also interested in the tail of the resolution. The study of the resolution tails is important; the small hypernuclear-production signal is not well separated in missing mass from the large signal of free Ξ^- production. The background under the hydrogen peak, consisting of Ξ^- production on carbon, is subtracted using the missing-mass spectrum of the carbon target. The resulting background-subtracted spectrum is shown in Fig. 4. The width of the peak from a Gaussian fit is 3.8 MeV/c^2 rms. It can be seen from the plot that the resolution is reasonably close to being Gaussian. The missing mass resolution for the 13 cm $\mathrm{CH_2}$ target was measured to be 4.2 MeV/c^2 rms for hydrogen kinematics.

The mass resolution is a function of the target mass. The resolution specific to Ξ^- production on hydrogen (which we measure directly) was used to infer the missing-mass resolution for carbon kinematics using simple kinematical considerations. A factor of 1.45 relates the missing-mass resolutions in carbon and hydrogen kinematics. This value results in a missing-mass resolution for carbon kinematics of 4.2 $\mathrm{MeV}/c^2 \times 1.45 = 6.1 \ \mathrm{MeV}/c^2$. The peak of Ξ^- production on hydrogen was also used for the energy-scale calibration. The position of the peak was adjusted to be at the Ξ^- mass value and the accuracy of the energy-scale calibration for the diamond target was estimated to be better than 0.5 MeV.

V. COMPARISON OF THE DATA AND THEORY

The theoretical (K^-, K^+) double differential cross section for $^{12}_{\Xi}\mathrm{Be}$ production, $d^2\sigma(\theta)/d\Omega_L dE_\Xi$, was calculated, for both bound and unbound Ξ^-s, in the Kapur-Peirls framework which was developed originally for an estimate of the (π^+, K^+) strength function [8]. The DWIA calculation was performed for a K^- momentum of 1.8 GeV/c by assuming the K-N elementary cross sections: $\sigma(K^-N) = 2.90 \ \mathrm{fm}^2$ and $\sigma(K^+N) = 1.99 \ \mathrm{fm}^2$. Further details of the calculation can
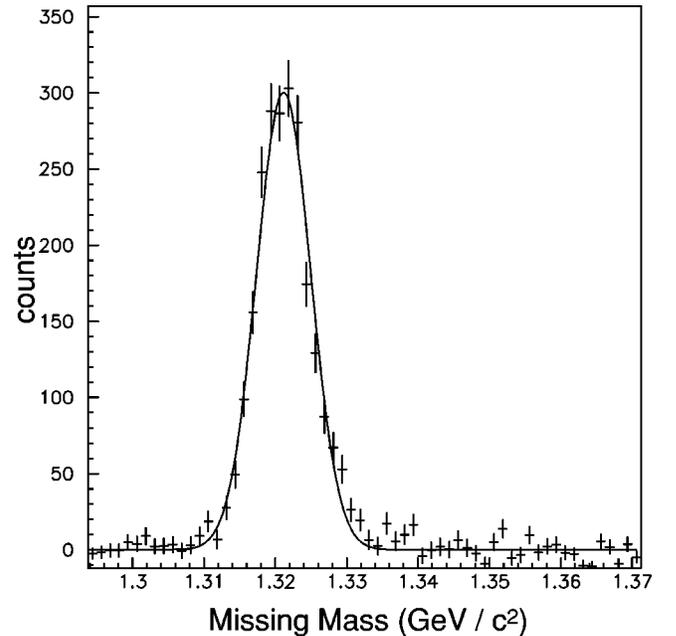

FIG. 4. Missing mass for Ξ^- production on hydrogen in the 8 cm long $\mathrm{CH_2}$ target. Background from reactions on carbon has been subtracted using a data sample, properly normalized, taken with diamond target. The solid line shows the best Gaussian fit.
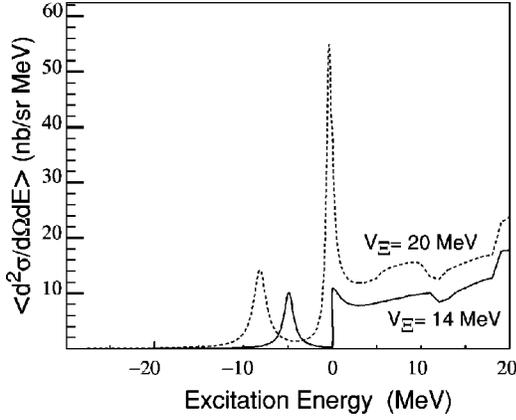
FIG. 5. Results of DWIA calculations, before folding by the experimental energy resolution, for the $^{12}C(K^-,K^+)^{12}_\Xi Be$ reaction for $V_{0\Xi}=14$ MeV and 20 MeV. The cross section has been averaged over the kaon angular range $0<\theta_{K^+}<14°$.

be found in the recent references [2,9] in which the (K^-,K^+) cross sections for the ^{12}C and ^{16}O targets have been estimated for $p_{K^-}=1.6$ GeV/c.

The calculation was performed for $0°<\theta_{K^+}<16°$ and a series of Woods-Saxon Ξ^- well depth parameter values: $V_{0\Xi}=12, 14, 16, 18,$ and 20 MeV. The radius and skin depth of the Ξ potential were fixed at $R=1.1A^{1/3}$ fm and $a_\Xi=0.65$ fm. The proton wave function in the ^{12}C target was generated using a Woods-Saxon potential with $V_{0N}=50$ MeV, $R=1.1A^{1/3}$ fm, and $a_N=0.65$ fm. The elementary Ξ^- production cross section was set to 35 μb/sr to be compatible with the normalization of our experimental data. The kinematic factor α, which accounts for the transformation between the two-body and A-body frames, was set to 0.73.

As a typical example of the angular dependence of the differential cross section, the dashed line in Fig. 3 shows the case of the ground state for $V_{0\Xi}=14$ MeV. In order to make a comparison between the theory and the data, we calculate the angle-averaged differential cross sections, $\langle(d^2\sigma/d\Omega dE)(E)\rangle$ and fold the results with the experimental resolution. However, we first present theoretical $^{12}C(K^-,K^+)^{12}_\Xi Be$ spectra which have not been folded by the experimental energy resolution but have been angle-averaged over $0°<\theta_{K^+}<14°$. As shown in Fig. 5, the result for $V_{0\Xi}=20$ MeV (dashed line) has two bound-state peaks, corresponding to the $\Xi^- s-$ and p-orbitals. The widths of these peaks are determined using a one-boson-exchange model to estimate the rate for the $\Xi N \rightarrow \Lambda\Lambda$ conversion. For the case of $V_{0\Xi}=14$ MeV, the p state is not bound but it is calculated as a resonance state in the continuum; therefore a sudden rise is seen just above the threshold in Fig. 5.

Figure 6 shows experimental excitation energy histograms for $^{12}C(K^-,K^+)X$ for two different limits on the scattering angle of the outgoing K^+, $\theta_{K^+}<14°$, and $\theta_{K^+}<8°$. The data clearly show an enhancement around zero excitation energy when compared to a Monte Carlo simulation based on quasifree Ξ production which has been normalized to the total number of $^{12}C(K^-,K^+)X$ events (curve QF).
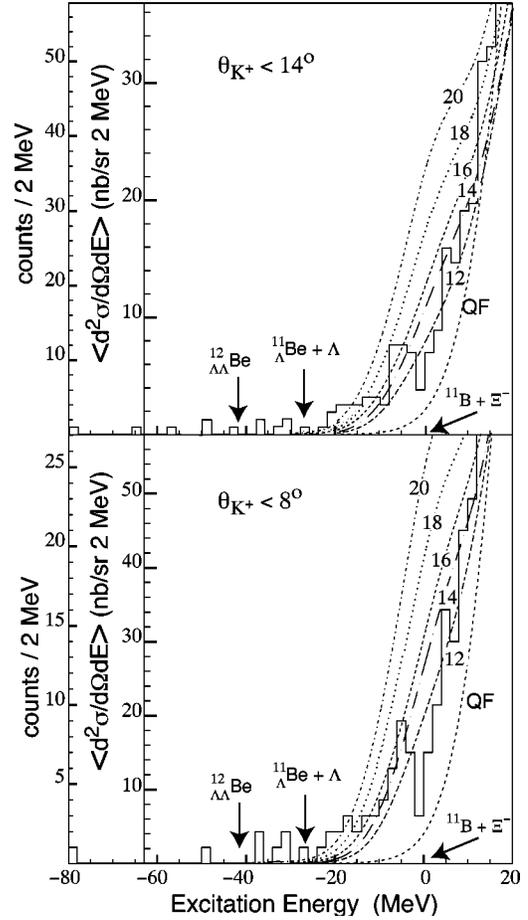

FIG. 6. Excitation-energy spectra from E885 for $^{12}C(K^-,K^+)X$ for $\theta_{K^+}<14°$ (top figure) and $\theta_{K^+}<8°$ (bottom figure) along with $^{12}_\Xi Be$ production theoretical curves for $V_{0\Xi}$ equal to 20, 18, 16, 14, and 12 MeV. The results of a quasifree Ξ production calculation are also shown (curve QF). The expected location of the ground state of $^{12}_{\Lambda\Lambda}Be$ and the thresholds for $^{11}_\Lambda Be+\Lambda$ and $^{11}B+\Xi^-$ production are indicated with arrows.

In the same figure, the $^{12}_\Xi Be$ production theoretical curves for several Ξ potential well depths, folded with the 6.1 MeV rms experimental resolution, are shown for comparison with the data. The expected location of the ground state of $^{12}_{\Lambda\Lambda}Be$ (assuming a total binding energy of the Λ's, $B_{\Lambda\Lambda}$, of 25 MeV) and the thresholds for $^{11}_\Lambda Be+\Lambda$ and $^{11}B+\Xi^-$ production are indicated. The normalization calculation for the case $\theta_{K^+}<8°$ is less sensitive to the model of angular dependence because the spectrometer acceptance is fairly flat over this region but drops rapidly for $\theta_{K^+}>8°$ as shown in Fig. 3; we present the results for both the entire acceptance and for $\theta_{K^+}<8°$ in Fig. 6.

Visual inspection shows that the theoretical curve for the value of the Ξ-nucleus potential well depth $V_{0\Xi}=14$ MeV agrees with the data reasonably well in the region of excitation energy -20 MeV$<E<0$ MeV and much better than the curve for $V_{0\Xi}=20$ MeV. If any of the observed signal results from direct two-Λ production without an intermediate $^{12}_\Xi Be$ state, the discrepancy between the $V_{0\Xi}=20$ MeV results and the remaining experimental signal becomes even

TABLE II. The experimental results integrated over the excitation energy -20 MeV$<E<0$ MeV are shown. The theoretical values for the averaged differential cross sections, after convoluting with the experimental resolutions and integrating over the same energy range, are shown as a function of the Ξ-nucleus potential well depth parameter, $V_{0\Xi}$. The corresponding values for the KEK E224 experiment [3], $p_{K^-}=1.66$ GeV/c, are shown where available.

	This work		KEK E224
	$\theta_{K^+}<8°$	$\theta_{K^+}<14°$	
Counts	42	67	3
Sensitivity (counts per nb/sr)	0.47	1.6	0.05
$\langle d\sigma/d\Omega\rangle$ Experiment (nb/sr)	89 ± 14	42 ± 5	60 ± 45
$\langle d\sigma/d\Omega\rangle V_{0\Xi}=12$ MeV (nb/sr)	67	26	
$\langle d\sigma/d\Omega\rangle V_{0\Xi}=14$ MeV (nb/sr)	92	37	
$\langle d\sigma/d\Omega\rangle V_{0\Xi}=16$ MeV (nb/sr)	115	46	75
$\langle d\sigma/d\Omega\rangle V_{0\Xi}=18$ MeV (nb/sr)	166	68	
$\langle d\sigma/d\Omega\rangle V_{0\Xi}=20$ MeV (nb/sr)	226	93	170

larger. The comparison of data to theory in the bound region can be quantified by considering the results for the angle-averaged cross section integrated over the -20 MeV$<E$ <0 MeV excitation region. The results are presented in Table II. It can be seen that the DWIA calculation predicts a yield more than a factor of two larger than the measured cross section in this region when a Ξ-nucleus potential well depth of 20 MeV is used.

VI. BACKGROUND

Events due to Ξ production off the hydrogen contained in the target and target-area scintillators produce a small peak at $\approx +90$ MeV in excitation energy; this peak represents only a few percent of the total events and thus this contamination does not affect the analysis near zero excitation energy. Background in the region of negative values of excitation energy can be divided into two groups. One group contributes a flat background caused by particle misidentification, severe tracking errors, etc. Such background might have some structure over a wider region of missing mass, but on a small, ≈ 100 MeV scale, it should be flat. This was confirmed when observing the background in the bound region obtained by using a loose set of cuts (hence considerable background contamination). The second group is due to leakage from $E>0$ due to finite missing-mass resolution.

Background of the first kind can be easily estimated by observing the region further below zero where leakage becomes negligible. There are 6 events in the interval of excitation energy $[-80$ MeV, -40 MeV$]$ for $\theta_{K^+}<14°$ (see Fig. 6). Since the flatness of the background was confirmed by loosening the cuts, an extrapolation can be made that the number of background events of the first kind in the excitation-energy region $[-20$ MeV, 0 MeV$]$ is about 3. It can be concluded then that the background of the first kind contributes only a small fraction of the total signal in the Ξ hypernuclear production region, and it is ignored when comparing the data to theory.

Background of the second kind is taken into account when the theoretical cross section is folded with the experimental resolution. The number of events in the $E<0$ region that leak from the $E>0$ region depends on the shape and magnitude of the excitation-energy spectrum for $E>0$ and on the resolution function shape. We found that the signal observed in the bound region cannot be explained by leakage from the $E>0$ region. This is already evidenced by the good agreement between the data and theory for $V_{0\Xi}=14$ MeV in the $E<0$ region, since non-zero cross section of hypernuclear production is essential to explain the events in the bound region. We, however, made two additional checks to demonstrate it. First, a Monte Carlo excitation-energy spectrum, where only free Ξ^- production is simulated and no events in the $E<0$ region are produced, was folded with the measured experimental resolution. It was found that only ≈ 10 events are expected to have $E<0$ for $\theta_{K^+}<14°$ (the observed number is 67). Second, a different resolution function was tried with very large tails added to the basic Gaussian resolution function. Even with those large tails, which are clearly ruled out by the resolution measurement, the signal in the bound region due to leakage was still a few times below the observed level.

VII. CONCLUSIONS

The measurement of the missing mass in the (K^-,K^+) reaction on carbon in E885 allowed the determination of the excitation-energy spectrum of directly produced $S=-2$ systems. The signal in the missing-mass region below the threshold for free Ξ^- production was examined in order to extract information on the existence of Ξ hypernuclei and the strength of the Ξ-nucleus potential. Our analysis has shown that the events in the bound region of the missing-mass spectrum could not be explained by non-$S=-2$ background or effects of limited resolution, and these events are consistent with hypernuclear production. Possible sources of the signal in the bound region are the production of one or two Λs in the continuum or double-Λ hyperfragments. The threshold for $^{11}_{\Lambda}$Be$+\Lambda$ is estimated to be at $E\approx -27$ MeV. This channel may dominate the other two-Λ channels since the two-step $(K^-,\pi),(\pi,K^+)$ process involves one low-momentum Λ and one high-momentum Λ. Its cross section is expected to be several orders of magnitude larger than the production cross section for double-Λ hypernuclei [10,11]. No quantitative estimate of the contribution of these processes in this kinematic regime has been made and final interpretation of the excitation spectrum in terms of one-step Ξ-hypernuclear production verses two-Λ production without an intermediate Ξ-state requires additional theoretical work.

A comparison of the data and the theoretical calculations for the cross sections of Ξ hypernuclear production, folded with the experimental resolution, shows a reasonable agreement of the data and theory for $V_{0\Xi}=14$ MeV in the region of excitation energy -20 MeV$<E<0$ MeV and a significant disagreement between the data and theory for $V_{0\Xi}=20$ MeV. These results are consistent with the conclusions of Ref. [3]. If a significant portion of the events in this region correspond to two-Λ production without an intermediate Ξ

hypernucleus, the discrepancy between the calculation using this well depth and our results would be even larger. We conclude that the results are consistent with the theoretical predictions when a potential depth of 14 MeV or less is assumed.

The accuracy of DWIA, which was used for the cross section calculation, was nominally assumed to be 30% in Ref. [3]. Although the DWIA framework has been successful in describing the production of single-Λ hypernuclei using the (π^+, K^+) and (K^-, π^-) reactions, it is possible that the DWIA accuracy for the (K^-, K^+) reaction is worse due to the higher momentum transfer. Therefore a value for the Ξ-nucleus potential well depth as high as 20 MeV, though less favored, cannot be completely ruled out. Additional the-

oretical calculations of the complete $^{12}C(K^-, K^+)X$ excitation spectrum are needed to determine the parameter space that is compatible with our results.

[1] C. B. Dover and A. Gal, Ann. Phys. (N.Y.) **146**, 309 (1983).

[2] Y. Yamamoto, T. Motoba, T. Fukuda, M. Takahashi, and E. Ikeda, Prog. Theor. Phys. Suppl. **117**, 281 (1994).

[3] T. Fukuda *et al.*, Phys. Rev. C **58**, 1306 (1998).

[4] D. E. Alburger and M. May, Nucl. Instrum. Methods Phys. Res. A (to be published).

[5] P. H. Pile *et al.*, Nucl. Instrum. Methods Phys. Res. A **321**, 48 (1992).

[6] R. W. Stotzer *et al.*, Phys. Rev. Lett. **78**, 3646 (1997).

[7] T. Iijima *et al.*, Nucl. Phys. **A546**, 588 (1992).

[8] T. Motoba, H. Bandō, R. Wünsch, and J. Žofka, Phys. Rev. C **38**, 1322 (1988).

[9] K. Ikeda, T. Fukuda, T. Motoba, M. Takahashi, and Y. Yamamoto, Prog. Theor. Phys. **91**, 747 (1994).

[10] C. B. Dover, Nukleonik **25**, 521 (1980).

[11] R. E. Chrien, C. B. Dover, and A. Gal, J. Czech. Phys. **42**, 1089 (1992).